JACS
JOURNAL OF THE AMERICAN CHEMICAL SOCIETY

ARTICLE

pubs.acs.org/JACS

Semi-metallic Single-Component Crystal of Soluble La@C_{82} Derivative with High Electron Mobility

Satoru Sato,[†] Shu Seki,[†,‡] Yoshihito Honsho,[‡] Lu Wang,[§] Hidefumi Nikawa,[†] Guangfu Luo,[§] Jing Lu,[†,∥] Masayuki Haranaka,[†] Takahiro Tsuchiya,[†] Shigeru Nagase,[†,§] and Takeshi Akasaka[†,*]

[†]Tsukuba Advanced Research Alliance, University of Tsukuba, Tsukuba, Ibaraki 305-8577, Japan

[‡]Department of Applied Chemistry, Graduate School of Engineering, Osaka University, Suita, Osaka 565-0871, Japan

[§]Department of Theoretical and Computational Molecular Science, Institute for Molecular Science, Okazaki, Aichi 444-8585, Japan

[∥]State Key Laboratory of Mesoscopic Physics and Department of Physics, Peking University, Beijing 100871, People's Republic of China

Supporting Information

ABSTRACT: We prepared an organic conductor crystal having extremely high electron mobility, in which the adamantylidene (Ad) derivative of La@C_{82} (an endohedral metallofullerene known as a n-type semiconductor) is aligned in an orderly fashion. The single-component crystal exhibits high electron mobility of $\mu > 10\ cm^2\ V^{-1}\ s^{-1}$ along the *c* axis under normal temperatures and pressures in the atmosphere, as shown by flash-photolysis time-resolved microwave conductivity (TRMC) measurements, which are the highest of reported organic conductors measured by TRMC. According to density functional calculations, the single crystal of La@C_{82}Ad is semi-metallic, with a small band gap of 0.005 eV.

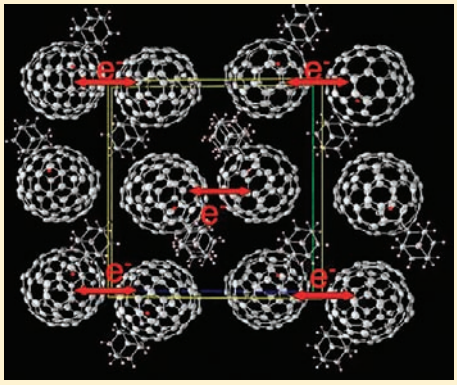

INTRODUCTION

Nanostructures with well-controlled composition and crystallinity are fascinating because of their structure−property relations and scientific and technological applications attributable to their dimensional anisotropy.[1] The research field of nanoscale organic electronics has received broad attention because of its operating principles and valuable fabrication techniques of nanoscale materials.[2] To date, several organic conducting materials[3−7] have become known, with charge-carrier mobilities determined as 4.1×10^{-4} −2.4 $cm^2\ V^{-1}\ s^{-1}$ using the time-resolved microwave conductivity (TRMC) measurement.[6,7] The TRMC measurement has served as an electodeless measurement tool for the determination of the intrinsic charge-carrier mobility in conjugated organic materials.[4] Meanwhile, endohedral fullerenes have attracted interest as new spherical molecules with unique structures and properties that are unexpected for empty fullerenes.[8] Endohedral metallofullerenes have attracted special interest as building blocks of future nanoscale electronic devices and conducting materials because they have low oxidation and reduction potentials.[9] Although the formation of crystals of endohedral metallofullerenes remains difficult, chemical derivatization allows for their efficient crystallization.[10] Herein, we investigate the charge-carrier mobilities of the single crystal and other molphorogies of the La@C_{82}Ad derivative[11] by TRMC and time-of-flight (TOF)[12] measurements.

EXPERIMENTAL SECTION

The La@C_{82}Ad derivative was synthesized using the regioselective reaction of La@C_{82} with 2-adamantane-2,3-[3*H*]-diazirine.[11] The isolated La@C_{82}Ad was dissolved in CS_2 and crystallized, evaporating the solution slowly at low temperature. The nanorods of La@C_{82}Ad were prepared by layering a solution of La@C_{82}Ad in CS_2 with 2-propanol at room temperature. After the two layers became homogeneous, needle-like precipitates (La@C_{82}Ad nanorods) were obtained. The La@C_{82}Ad nanorods were characterized as single-crystal-morphous.[13] The C_{60}Ad (5,6-adduct) was prepared by the reported procedure.[14] To compare to the charge-carrier mobilities, the CS_2 solutions of La@C_{82}, La@C_{82}Ad, and C_{60}Ad were drop-casted onto the substrate.

TRMC Measurement. Nanosecond laser pulses from a Nd:YAG laser {INDY-HG [full width at half maximum (fwhm) of 5−8 ns], second harmonic generation (SHG) (532 nm) and third harmonic generation (THG) (355 nm); Spectra-Physics} were used as excitation sources. The laser power density was set to 0.1−30 mJ/cm^2 (0.09−5.1×10^{16} photons/cm^2). For TRMC measurements, the microwave frequency and power were set at approximately 9.1 GHz and 3 mW, respectively, so that the charge-carrier motion was not disturbed by the low electric field of the microwave. The TRMC signal picked up by a diode (rise time < 1 ns) is monitored using a digital oscilloscope. All

Received: November 21, 2010
Published: February 4, 2011

   dx.doi.org/10.1021/ja110465y | *J. Am. Chem. Soc.* 2011, 133, 2766–2771

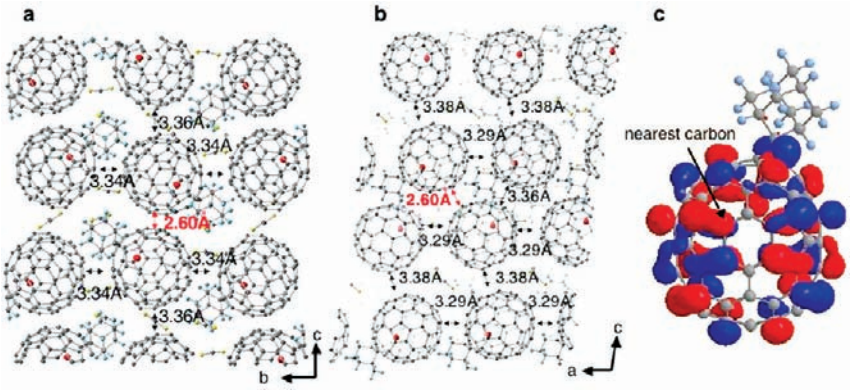

Figure 1. (a and b) Crystal structure of the La@C_{82}Ad single crystal. (c) LUMO of La@C_{82}Ad.

experiments described above were conducted at room temperature. The transient photoconductivity ($\Delta\sigma$) of the samples is related to the reflected microwave power ($\Delta P_r/P_r$) and the sum of mobilities of charge carriers as

$$\langle \Delta\sigma \rangle = \frac{1}{A}\frac{\Delta P_r}{P_r} \quad (1)$$

and

$$\Delta\sigma = eN\phi\sum\mu = eI_0F\varphi\sum\mu \quad (2)$$

where A, e, ϕ, N, $\sum\mu$, I_0, and F represent a sensitivity factor, the elementary charge of an electron, the photocarrier generation yield (quantum efficiency), the number distribution of absorbed photons per unit volume, the sum of mobilities for negative and positive carriers, the incident light intensity, and the spatial distribution factor of charge carriers wighted by the electric field strength in the cavity (filling factor), respectively.[3,15−17] Polarization of the laser pulses is isotropic. All crystals are mounted on quartz rods and overcoated with polysiloxane. The experimental setup is presented in Figure S1 in the Supporting Information. The number of photons absorbed by the crystals is estimated through direct measurement of the transmitted power of laser pulses through the (quartz rod)−(crystal with PMMA binder)−(quartz rod) geometry (Figure S1 in the Supporting Information) using an Opher NOVA-display laser power meter. The quartz rod is rotated in the microwave cavity. Then, the changes in the effective electric field in the crystals by the rotation of the samples are calculated numerically based on the geometry of the crystals captured using a digital charge coupled device (CCD) camera, leading to the negligible changes of the value of F = 3840−3860 m^{-1} (single crystal) and 8480−8520 m^{-1} (nanorod) for the measured values of $\Delta\sigma$. The error analysis of the final values of mobility was carried out on the basis of the errors in the numbers of photons absorbed in the crystals derived from the power meter and the estimate of the light scattering observed for the identical geometry of the quartz rods unmounted from the crystals.

The values of ϕ in the compounds were determined by a conventional photocurrent measurement in a vacuum chamber (<10^{-5} Pa) using interdigitated Au electrodes with a 5 μm gap under excitation at 355 or 532 nm with a power density of 4.1 × 10^{14}−5.4 × 10^{16} photons/cm^2. The transient current was observed predominantly under the applied bias of 0−20 V (ca. 0−4.0 × 10^4 V cm^{-1}) and monitored using a source meter (2612; Keithley Instruments, Inc.). The photocarrier generation yield was estimated from the $I-V$ traces under dark/355 (532) nm illumination conditions. Other details of the set of apparatus were described elsewhere.[5,12,18,19]

TOF Measurement. The photogenerated carrier drift mobility was measured using the current-mode TOF technique. The CS_2 solution of La@C_{82}, La@C_{82}Ad, and C_{60}Ad were drop-casted onto an Al substrate to 22−52 μm thickness. They were in turn sandwiched with a semi-transparent Au top electrode. The current transients were measured at 293 K after 12 h of annealing at 373 K under high vacuum conditions and photoexcited at the upper surface of film using a 337 nm pulse from the N_2 laser. The log−log plots of the current transient observed for drop-casted La@C_{82}, La@C_{82}Ad, and C_{60}Ad are presented in Figire S2 in the Supporting Information.

Characterization. To characterize the structure and morphology of La@C_{82}, La@C_{82}Ad, and C_{60}Ad drop-casted from CS_2 solution on the substrate, scanning electron microscopy (SEM) observations were carried out using a JSM-7001 of JEOL, Ltd. at 15.0 kV. Atomic force microscopy (AFM) and dynamic force microscopy (DFM) observations were carried out using a Nano-Navi II scanning probe microscope of SII-Nanotechnology, Inc. X-ray diffraction (XRD) patterns were taken on PANalytical X'Pert Pro MPD with Cu Kα radiation (λ = 1.542 Å), operating at 45 kV and 40 mA. The XRD sample was prepared by depositing a sample in CS_2 solution on a nonreflective substrate.

RESULTS AND DISCUSSION

The single crystal of La@C_{82}Ad was prepared by evaporating the solution slowly at low temperature. The crystal structure that was determined is shown in panels a and b of Figure 1.

To determine the transient conductivity, the TRMC measurement of the single crystal of La@C_{82}Ad was conducted. Its anisotropy was observed by rotating the sample stage relative to the direction of the microwave electronic field in the resonant cavity. As Figure 2 shows, the maximum value of the transient conductivity ($\phi\sum\mu$) reaches 3.5 ± 0.5 × 10^{-3} cm^2 V^{-1} s^{-1} along the c axis, where ϕ and $\sum\mu$ denote the photocarrier generation yield (quantum efficiency) and the sum of mobilities for positive and negative charge carriers, respectively. In contrast, the single crystal shows the considerably smaller transition conductivities of 1.2 ± 0.2 × 10^{-3} and 6.5 ± 1.0 × 10^{-4} cm^2 V^{-1} s^{-1} along the direction making 45° and 90° angles to the c axis, respectively. This anisotropy is attributable to the presence of the Ad group and packed CS_2 molecules, both of which serve as an insulating part and might be effectively applicable to molecular electronics. For comparison, TRMC measurements were performed for the drop-casted La@C_{82}Ad. The $\phi\sum\mu$ value of 7.0 ± 1.0 × 10^{-5} cm^2 V^{-1} s^{-1} for the drop-casted La@C_{82}Ad (Figure 3) is much smaller than that of 3.5 × 10^{-3} cm^2 V^{-1} s^{-1} for the single crystal, which indicates that single crystallization is important, giving the orderly aligned La@C_{82}Ad. The TRMC measurement of La@C_{82}Ad nanorods was also conducted to

dx.doi.org/10.1021/ja110465y |J. Am. Chem. Soc. 2011, 133, 2766–2771

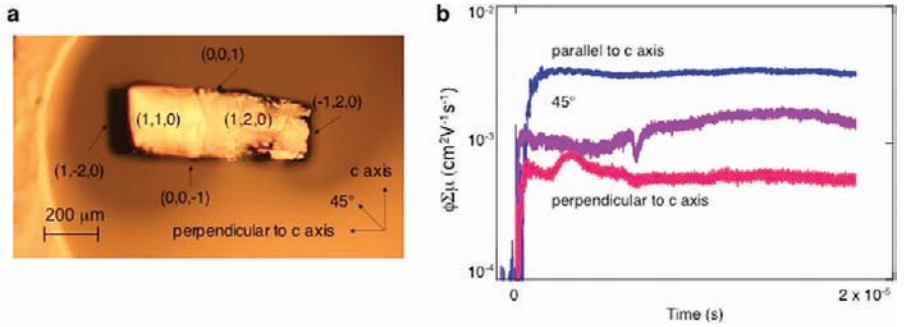

Figure 2. (a) Photograph and (b) observed transient conductivity for single-crystal La@C_{82}Ad. Excitation was conducted at 532 nm: 10 mJ/cm^2.

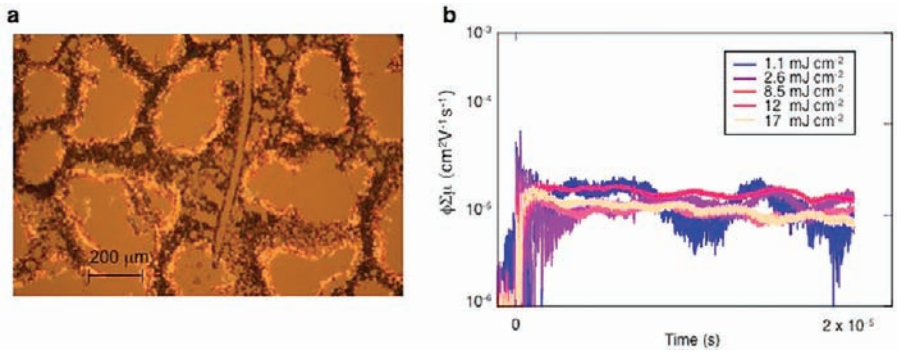

Figure 3. (a) Photograph and (b) observed transient conductivity for drop-casted La@C_{82}Ad. Excitation was conducted at 532 nm: 1.1−17 mJ/cm^2.

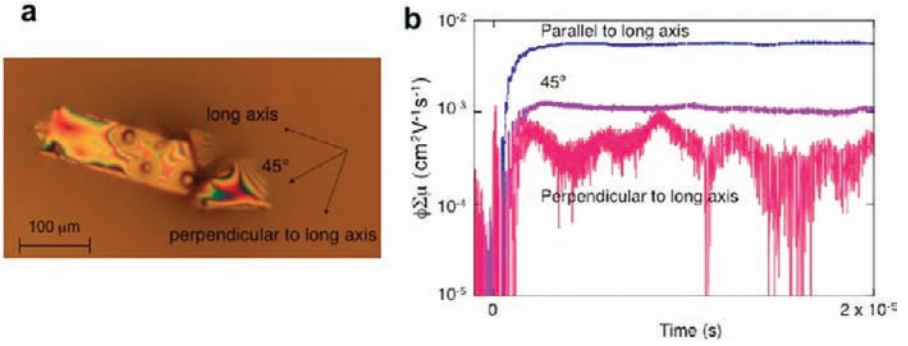

Figure 4. (a) Photograph and (b) observed conductivity transients for nanorods of La@C_{82}Ad. Excitation was conducted at 532 nm: 45 mJ/cm^2.

examine the charge-carrier mobility (Figure 4). The anisotropic mobility of La@C_{82}Ad nanorods was investigated by rotating the sample stage relative to the direction of the microwave electronic field in the resonant cavity. The maximum value of the conductivity transient ($\phi\sum\mu$) reaches $5.7 \pm 1.0 \times 10^{-3}$ cm^2 V^{-1} s^{-1} along the long axis. In contrast, the $\phi\sum\mu$ values along the direction making 45° and 90° angles to the long axis were found to be smaller ($1.2 \pm 0.2 \times 10^{-3}$ and $8.0 \pm 1.0 \times 10^{-4}$ cm^2 V^{-1} s^{-1}, respectively). The transient conductivity of the La@C_{82}Ad single crystal shows the anisotropy (e.g., the $\phi\sum\mu$ values of along the *c* axis and perpendicular to the *c* axis direction are 3.5×10^{-3}, 1.2×10^{-3}, and 6.5×10^{-4} cm^2 V^{-1} s^{-1}, respectively), resembling the tendency of La@C_{82}Ad nanorods, which might indicate that the directions revealing the maximum transient conductivity in nanorods and a single crystal of La@C_{82}Ad have the same molecular alignment, such that the long axis of La@C_{82}Ad nanorods has a similar crystal alignment to that of the *c* axis of the La@C_{82}Ad single crystal. Therefore, the obtained values reveal a similar scale.

To discern the charge carrier, the transient conductivity for the drop-casted La@C_{82}Ad was investigated under O_2, SF_6, and Ar atmospheres. The $\phi\sum\mu$ values of $2.0 \pm 0.3 \times 10^{-5}$ and $1.7 \pm 0.2 \times 10^{-5}$ cm^2 V^{-1} s^{-1} under air (20% O_2) and SF_6 atmospheres are smaller than that of $3.0 \pm 0.4 \times 10^{-5}$ cm^2 V^{-1} s^{-1} under an Ar atmosphere (Figure 5) with the faster decay rates. The smaller values under O_2 and SF_6 suggest that electrons are responsible for the charge carrier because O_2 and SF_6 act as electron-quenchers.

To determine the yield of the photocarrier generation, a photocurrent measurement was performed for the drop-casted La@C_{82}Ad onto an Au interdigitated electrode, as shown in Figure 6. In the range of the light excitation at 4.1×10^{14}−5.4×10^{16} cm^{-2},

dx.doi.org/10.1021/ja110465y |*J. Am. Chem. Soc.* 2011, 133, 2766–2771

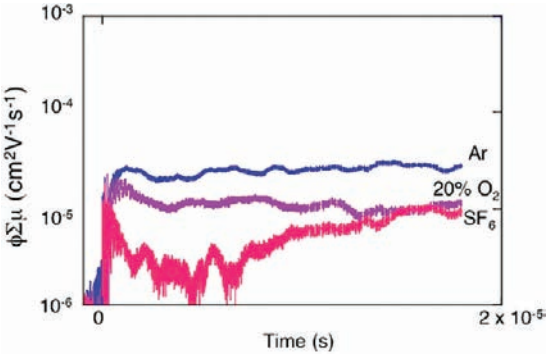

Figure 5. Observed transient conductivity monitored for drop-casted La@C_{82}Ad under various gas atmospheres. Excitation was conducted at 532 nm: 8.7 (Ar), 8.4 (20% O_2), and 7.9 (SF_6) mJ/cm^2.

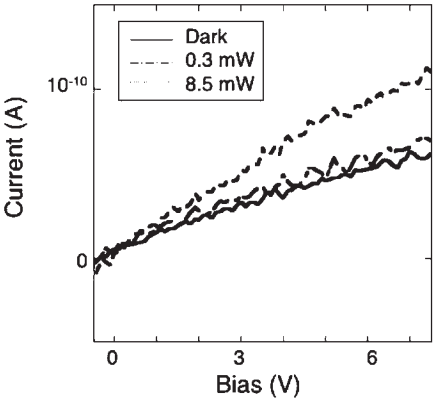

Figure 6. $I-V$ characterization of a drop-casted La@C_{82}Ad onto an Au interdigitized electrode with a 5 μm gap. Illumination was conducted at 532 nm.

the linear $I-V$ traces were observed and the derived conductance was also proportional to the excitation. Thus, integration of the transient current engenders the maximum yield of $\phi \approx 1.0 \pm 0.4 \times 10^{-3}$ for photocarrier generation under the applied bias, which is unusually higher than the yield of free-charge generation in the conjugated organic crystals because of the high electric field strength in this measurement. Using the maximum yield, the electron mobility of the single crystal along the c axis is evaluated as at least $\mu = 10 \pm 5$ cm^2 V^{-1} s^{-1}. It is notable that the value is the largest of reported organic conductors measured by TRMC. On the other hand, the corresponding electron mobility is 2 ± 1 and $7 \pm 3 \times 10^{-1}$ cm^2 V^{-1} s^{-1} for the single crystal along the direction, making 45° and 90° angles to the c axis, respectively, whereas it is $\mu = 7 \pm 3 \times 10^{-2}$ cm^2 V^{-1} s^{-1} for the drop-casted La@C_{82}Ad and $\mu > 10$ cm^2 V^{-1} s^{-1} for the La@C_{82}Ad nanorods along the long axis. As Figure 6 shows, the single crystal of La@$_{82}$Ad exhibits a considerable dark current in the $I-V$ trace measurement, suggesting that the single crystal works as an organic conductor without light irradiation.

To provide theoretical insight into the single crystal of La@C_{82}Ad, local density functional calculations were performed using the DMol^3 code.[20] No significant deformation from the experimental structure was found by geometry optimization. The band structure calculated for the optimized structure is presented in Figure 7. The energy difference between the valence-band top and the conduction-band bottom (band gap) is only 0.005 eV

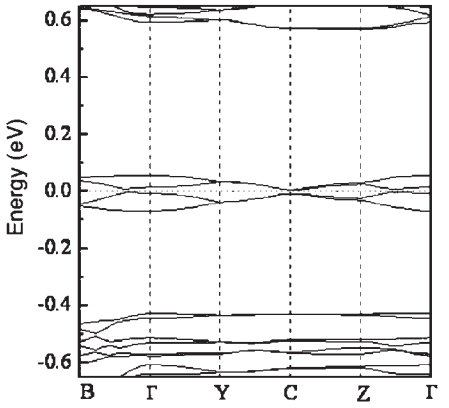

Figure 7. Band structure of the La@C_{82}Ad single crystal.

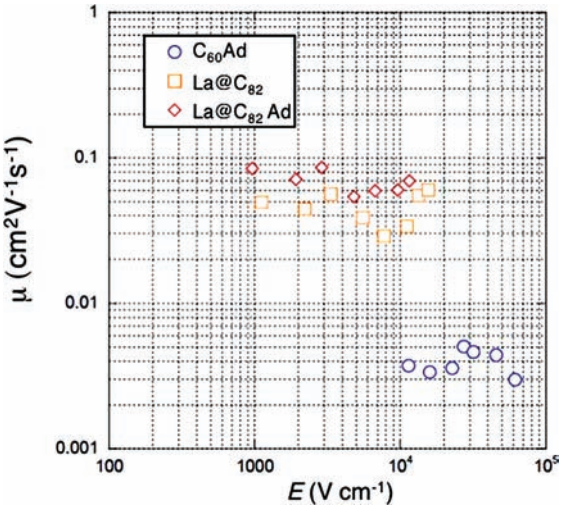

Figure 8. Dependence of mobility upon electronic field strength in negative-bias mode observed for La@C_{82}, La@C_{82}Ad, and C_{60}Ad.

from our calculation. In general, the conductivity of semiconductors is strongly dependent upon the band gap. At room temperature, the La@C_{82}Ad single crystal has significant valence electrons, which have enough thermal energy, excited across the very small band gap to the conduction band. This provides sufficient electron and hole carriers in the crystal. Thus, the La@C_{82}Ad single crystal can be regarded as a semi-metal and has high conductivity. The calculated effective mass of the carrier near the Fermi level is provided in Figure S3 in the Supporting Information. The effective mass of electron of the conduction-band bottom and hole of the valence-band top is 0.97 and 0.91m_0 (where m_0 is the mass of free electron), respectively, suggestive of nearly free-electron behavior. The shortest interatomic distance between the La@C_{82}Ad units is 2.60 Å (panels a and b of Figure 1). The lowest unoccupied molecular orbital (LUMO) of La@C_{82}Ad has a large distribution on the nearest carbon atoms (Figure 1c) and contributes to the electron mobility. Because the distance between fullerenes as well as the LUMO character is changeable using various derivatives of endohedral metallofullerenes, the band gap and carrier concentration are tunable.

In an attempt to examine the effect of endohedral La-doping, the drift mobilities of La@C_{82} and La@C_{82}Ad deposited on the substrate were compared to that of C_{60}Ad using the TOF

dx.doi.org/10.1021/ja110465y |J. Am. Chem. Soc. 2011, 133, 2766–2771

measurement (Figure 8). For this purpose, La@C_{82}, La@C_{82}Ad, and C_{60}Ad were dissolved into the CS_2 solution and casted on the substrates at 45, 52, and 22 μm thickness, respectively. The current transients were observed exclusively under the negative bias, supporting the electrons also being the major charge carriers in all of these compounds. The transient currents were measured at 293 K after 12 h annealing at 373 K under high vacuum conditions ($<10^{-5}$ Pa). The dependence of the mobility upon the electron field strength in negative-bias mode was observed, suggesting that the charge carriers are electrons. The electron drift mobilities of the drop-casted La@C_{82} and La@C_{82}Ad were estimated as $6.0 \pm 2.0 \times 10^{-2}$ and $8.0 \pm 2.4 \times 10^{-2}$ $cm^2\ V^{-1}\ s^{-1}$, respectively. These values are 1 order of magnitude higher than the $5.0 \pm 1.5 \times 10^{-3}$ $cm^2\ V^{-1}\ s^{-1}$ value estimated for C_{60}Ad, indicating the importance of endohedral La-doping in enhancing the mobility.

To characterize the morphology of La@C_{82}, La@C_{82}Ad, and C_{60}Ad drop-casted from a CS_2 solution on the substrate, XRD, SEM, and AFM measurements were carried out. The XRD measurement displayed some sharp reflections, suggesting that these samples had crystalline structures, respectively (Figure S4 in the Supporting Information). Figures S5 and S6 in the Supporting Information show the SEM micrographs and topographic/phase images in AFM measurements of La@C_{82}, La@C_{82}Ad, and C_{60}Ad drop-casted on the substrate, respectively. Polycrystalline features are typically observed in the SEM micrographs of La@C_{82}Ad, which is in contrast to the partially amorphous nature of the casted films of La@C_{82} and C_{60}Ad. This is also confirmed by the AFM images, showing the presence of microcrystalline domains in La@C_{82} and C_{60}Ad films observed as the phase contrast in the images. This is the case giving the highest values of mobility in the La@C_{82}Ad films determined as the long-range translational motion of electrons in the TOF measurement.

CONCLUSION

In conclusion, we found that the single crystal of the La@C_{82}Ad derivative exhibits a high electron mobility of 10 $cm^2\ V^{-1}\ s^{-1}$ and semi-metallic property. Because the La@C_{82}Ad derivative is soluble in many solvents,[21] it is applicable to device integration, unlike insoluble amorphous silicon, rubrene,[22] pentacene,[23] [Ni(tmdt)$_2$] (tmdt = trimethylenetetrathiafulvalenedithiolate),[24] and graphene.[25] Because the distance between fullerenes and the electronic property are controllable by changing the Ad part and the endohedral La atom, the band gap and carrier concentration are tunable. This La@C_{82}Ad derivative has a high potential as one of the candidates for new organic semiconductors. It is expected that the derivatization of endohedral metallofullerene will open up a new field related to tunable organic conductors for molecular electronics.

ASSOCIATED CONTENT

Supporting Information. Complete refs 11, 13, and 18; schematic showing the setup of the TRMC measurement; results of TOF measurements; calculated band structure and effective mass of the carrier near the Fermi level; XRD patterns, SEM images, AFM images, and DFM images for drop-casted La@C_{82}, La@C_{82}Ad, and C_{60}Ad; and examples of charge-carrier mobilities for organic conducting materials. This material is available free of charge via the Internet at http://pubs.acs.org.

AUTHOR INFORMATION

Corresponding Author
akasaka@tara.tsukuba.ac.jp

ACKNOWLEDGMENT

This work was supported in part by a Grant-in-Aid for Scientific Research on Innovation Areas (20108001, "pi-Space"), a Grant-in-Aid for Scientific Research (A) (20245006), The Next Generation Super Computing Project (Nanoscience Project), Nanotechnology Support Project, Grants-in-Aid for Scientific Research on Priority Area (20036008 and 20038007), and Specially Promoted Research from the Ministry of Education, Culture, Sports, Science, and Technology of Japan and The Strategic Japanese−Spanish Cooperative Program funded by JST and MICINN. We thank Prof. Toshiharu Teranishi, University of Tsukuba, for the XRD measurement. S.S. and H.N. thank the Japan Society for the Promotion of Science (JSPS) for Research Fellowships for Young Scientists.

REFERENCES

(1) (a) Li, R.; Hu, W.; Liu, Y.; Zhu, D. *Acc. Chem. Res.* **2010**, *43*, 529–540. (b) Zhang, H.; Wang, D.; Yang, B.; Möhwald, H. *J. Am. Chem. Soc.* **2006**, *128*, 10171–10180. (c) Cheng, J. Y.; Zhang, F.; Chuang, V. P.; Mayes, A. M.; Ross, C. A. *Nano Lett.* **2006**, *6*, 2099–2103. (d) Patzke, G. R.; Krumeich, F.; Nesper, R. *Angew. Chem., Int. Ed.* **2010**, *41*, 2446–2461. (e) Huang, Y.; Duan, X.; Wei, Q.; Lieber, C. M. *Science* **2001**, *291*, 630–633. (f) Hu, J.; Odom, T. W.; Lieber, C. M. *Acc. Chem. Res.* **1999**, *32*, 435–445.

(2) (a) Anthony, J. E. *Angew. Chem., Int. Ed.* **2008**, *47*, 452–483. (b) Cai, L.; Cabassi, M. A.; Yoon, H.; Cabarcos, O. M.; McGuiness, C. L.; Flatt, A. K.; Allara, D. L.; Tour, J. M.; Mayer, T. S. *Nano Lett.* **2005**, *5*, 2365–2372. (c) Duan, X.; Huang, Y.; Cui, Y.; Wang, J.; Lieber, C. M. *Nature* **2001**, *409*, 66–69. (d) Cui, Y.; Lieber, C. M. *Science* **2001**, *291*, 851–853.

(3) Grozema, F. C.; Siebbeles, L. D. A.; Warman, J. M.; Seki, S.; Tagawa, S.; Scherf, U. *Adv. Mater.* **2002**, *14*, 228–231.

(4) Saeki, A.; Seki, S.; Koizumi, Y.; Sunagawa, T.; Ushida, K.; Tagawa, S. *J. Phys. Chem. B* **2005**, *109*, 10015–10019.

(5) Amaya, T.; Seki, S.; Moriuchi, T.; Nakamoto, K.; Nakata, T.; Sakane, H.; Saeki, A.; Tagawa, S.; Hirao, T. *J. Am. Chem. Soc.* **2009**, *131*, 408–409.

(6) Li, W.; Yamamoto, Y.; Fukushima, T.; Saeki, A.; Seki, S.; Tagawa, S.; Masunaga, H.; Sasaki, S.; Takata, M.; Aida, T. *J. Am. Chem. Soc.* **2008**, *130*, 8886–8887.

(7) Tezuka, N.; Umeyama, T.; Seki, S.; Matano, Y.; Nishi, M.; Hirao, K.; Imahori, H. *J. Phys. Chem. C* **2010**, *114*, 3235–3247.

(8) (a) *Endofullerenes: A New Family of Carbon Clusters*; Akasaka, T., Nagase, S., Eds.; Kluwer Academic Publishers: Dordrecht, The Netherlands, 2002; pp 13−65. (b) *Chemistry of Nanocarbons*; Akasaka, T., Wudl, F., Nagase, S., Eds.; Wiley: London, U.K., 2010.

(9) Kobayashi, K.; Nagase, S. *Chem. Phys. Lett.* **1998**, *282*, 325–329.

(10) Yamada, M.; Akasaka, T.; Nagase, S. *Acc. Chem. Res.* **2010**, *43*, 93–102.

(11) Maeda, Y.; et al. *J. Am. Chem. Soc.* **2004**, *124*, 6858–6859.

(12) (a) Seki, S.; Yoshida, Y.; Tagawa, S.; Asai, K.; Ishigure, K.; Furukawa, K.; Fujiki, M.; Matsumoto, N. *Philos. Mag. B* **1999**, *79*, 1631–1645. (b) Kunimi, Y.; Seki, S.; Tagawa, S. *Solid State Commun.* **2000**, *114*, 469–472. (c) Shirota, Y.; Kageyama, H. *Chem. Rev.* **2007**, *107*, 953–1010.

(13) Tsuchiya, T.; et al. *J. Am. Chem. Soc.* **2008**, *130*, 450–451.

(14) Akasaka, T.; Liu, M. T. H.; Niino, Y.; Maeda, Y.; Wakahara, T.; Okamura, M.; Kobayashi, K.; Nagase, S. *J. Am. Chem. Soc.* **2000**, *122*, 7134–7135.

(15) Acharya, A.; Seki, S.; Saeki, A.; Koizumi, Y.; Tagawa, S. *Chem. Phys. Lett.* **2005**, *404*, 356–360.

(16) Saeki, A.; Seki, S.; Sunagawa, T.; Ushida, K.; Tagawa, S. *Philos. Mag.* **2006**, *86*, 1261–1276.
(17) Nagashima, K.; Yanagida, T.; Tanaka, H.; Seki, S.; Saeki, A.; Tagawa, S.; Kawai, T. *J. Am. Chem. Soc.* **2008**, *130*, 5378–5382.
(18) Imahori, H.; et al. *Chem.—Eur. J.* **2007**, *13*, 10182–10193.
(19) Hisaki, I.; Sakamoto, Y.; Shigemitsu, H.; Tohnai, N.; Miyata, M.; Seki, S.; Saeki, A.; Tagawa, S. *Chem.—Eur. J.* **2008**, *14*, 4178–4187.
(20) (a) Delley, B. *J. Chem. Phys.* **1990**, *92*, 508–517. (b) Delley, B. *J. Chem. Phys.* **2000**, *113*, 7756–7764.
(21) La@C_{82}Ad is dissolved in organic solvents used for treating fullerenes, such as CS_2, toluene, *o*-dichlorobenzene, etc. Its solubility is similar to pristine La@C_{82} (e.g., >0.3 mg/mL in CS_2). Furthermore, La@C_{82}Ad is kept without any change for at least 1 year under an argon atmosphere and light shielding conditions.
(22) Yamagishi, M.; Takeya, J.; Tominari, Y.; Nakazawa, Y.; Kuroda, T.; Ikehata, S.; Uno, M.; Nishikawa, T.; Kawase, T. *Appl. Phys. Lett.* **2007**, *90*, 182117.
(23) Jurchescu, O. D.; Baas, J.; Palstra, T. T. *Appl. Phys. Lett.* **2004**, *84*, 3061.
(24) Tanaka, H.; Okano, Y.; Kobayashi, H.; Suzuki, W.; Kobayashi, A. *Science* **2001**, *291*, 285–287.
(25) Novoselov, K. S.; Geim, A. K.; Morozov, S. V.; Jiang, D.; Zhang, Y.; Dubonos, S. V.; Grigorieva, I. V.; Firsov, A. A. *Science* **2004**, *306*, 666–669.